11th AIAA/CEAS Aeroacoustics Conference (26th AIAA Aeroacoustics Conference)
23 - 25 May 2005, Monterey, California

AIAA 2005-2890

PARAMETRIC STUDY OF FAN FLOW DEFLECTORS FOR JET NOISE SUPPRESSION

Dimitri Papamoschou *
University of California, Irvine, California 92697-3975

The paper provides an overview of a parametric study of fan flow deflectors (FFD) for jet noise suppression. Reductions in sideline and flyover noise at takeoff cycle point provide a total reduction in EPNL as high as 9.6 dB. Correlations of noise reduction versus the turning effort by the deflectors brings out some general trends and help identify promising configurations.

Introduction

This is continuation of experimental work at U.C. Irvine on fan flow deflection (FFD) [1]. The working principle of FFD is reduction of the convective Mach number of turbulent eddies that generate intense downward and sideward sound radiation. In a coaxial separate-flow turbofan engine this is achieved by tilting in the general downward direction, by a few degrees, the bypass (secondary) plume relative to the core (primary) plume. Mean flow surveys show that the misalignment of the two flows causes a thick, low-speed secondary core on the underside of the high-speed primary flow, especially in the region near the end of the primary potential core which contains the strongest noise sources. The secondary core reduces the convective Mach number of the primary eddies, thus hindering their ability to generate sound that travels to the downward acoustic far field [2]. Tilting of the bypass stream is possible by means of fixed or variable vanes installed near the exit of the bypass duct. Figure 1 depicts the general concept. Computational work has shown that the thrust penalty is on the order of 0.05% [3]. This paper describes a parametric study of FFD and some preliminary trends that have emerged.

Experimental Setup

Nozzle

The nozzle was a scaled-down version of the baseline separate-flow nozzle used in the Nozzle Acoustic Test Rig (NATR) of NASA Glenn Research Center [5]. The coordinates of the NATR nozzle were divided by a factor of eight to fit within the flow capacity of the UCI lab. Figure 2 plots the coordinates of the UCI nozzle. The nozzle was attached to a dual-stream apparatus that supplied mixtures of helium and air to the primary (core) and secondary (bypass) nozzles. Comparison of the UCI acoustic results with those from the NATR facility (which runs large-scale hot jets) shows excellent agreement in all aspects of noise [6]. The exit flow conditions, listed in Table 1, matched the typical exit conditions of a turbofan engine with bypass ratio 4.8 at takeoff setting. The Reynolds number of the jet, based on fan diameter, was 0.6×10^6.

Noise Measurement

Noise measurements were conducted inside an anechoic chamber using a one-eighth inch condenser microphone (Brüel & Kjær 4138) with frequency response of 140 kHz (Fig. 3). The microphone was mounted on a pivot arm and traced a circular arc centered at the jet exit with radius of $r = 0.96$ m. The polar angle θ ranged from 20° to 120° in intervals of 5° for $20° \leq \theta \leq 50°$ and 10° for the rest. Rotation of the nozzle assembly allowed variation of the azimuth emission angle, which took the values $\phi = 0°$ and $\phi = 60°$. The microphone was sampled at 400 kHz by a fast analog-to-digital board (National Instruments PCI-6070E) installed in a Pentium 4 computer. The narrowband power spectrum of the microphone voltage was computed using a 2048-point Fast Fourier Transform, which provided a spectral resolution of 195 Hz. The sound spectra were corrected for the microphone frequency response, free field response, and atmospheric absorption. Integration of the corrected spectrum yielded the overall sound pressure level (OASPL).

PNL time histories and Effective Perceived Noise Levels (EPNLs) were computed for flyover and sideline monitors at takeoff cycle point. For the procedure, the reader is referred to [1]. The aircraft con-

*Professor, Associate Fellow AIAA

sidered is twin-engine, each engine producing 90 kN of thrust (scale factor = 42). The flyover flight path is straight and level at an altitude of 460 m. Papamoschou [1] determined that the sideline EPNL for a typical initial climb profile can be approximated accurately by combining the flyover EPNL values from the acoustic measurements $\phi = 0°$ and 60° as follows:

$$\mathrm{EPNL_{sl}} = 0.15\mathrm{EPNL_{fo,0}} + 0.85\mathrm{EPNL_{fo,60}} - 2.2 \text{ dB}$$

The cumulative EPNL therefore is

$$\begin{aligned} \mathrm{EPNL_{cum}} &= \mathrm{EPNL_{fo,0}} + \mathrm{EPNL_{sl}} \\ &= 1.15\ \mathrm{EPNL_{fo,0}} + 0.85\ \mathrm{EPNL_{fo,60}} - 2.2 \text{ dB} \end{aligned}$$

We use an analogous definition for the cumulative OASPL, in a given polar direction:

$$\mathrm{OASPL_{cum}} = 1.15\ \mathrm{OASPL_0} + 0.85\ \mathrm{OASPL_{60}}$$

The reduction in cumulative EPNL is used here as a "figure of merit" for evaluating the noise reduction potential of FFD configurations. It does not necessarily correspond to the noise reduction from an actual airplane as this is influenced by many additional factors absent in our experiment (forward flight effect, engine installation effects, fan noise, airframe noise, etc).

Deflectors

This study encompassed the following categories of fan flow deflectors: single pair of vanes (2V), wedge (W), combination of single pair of vanes and wedge (2V+W) and two pairs of vanes (4V). They are shown in Fig. 4 with the pertinent geometric variables. The vanes were fabricated from thin (0.13-mm) brass sheet and were attached to the outer surface of the inner nozzle with adhesive. Electrical tape (0.18-mm thickness) was wrapped around the vanes to produce a round leading edge. The wedge deflectors were cut from 3.5-mm-thick nylon sheet. The height of the wedges matched approximately the height of the fan duct at the nozzle exit.

For the vane deflectors, the variables comprised: chord length, c; axial location of trailing edge relative to the exit of the nozzle, x_{te}; angle of attack, α; and azimuth angle, ϕ. For the wedge-type deflectors, the variables were: side length, ℓ; axial location of apex relative to the exit of the nozzle, x_{apex}; and wedge half-angle, α. All the wedges were mounted at the top of the nozzle ($\phi = 180°$.)

The parameter space is huge and cannot be covered completely with finite resources and in finite time. The approach taken here was to first discretize the parameters in values that seem reasonable from aerodynamic and practical points of view. Then we conducted a wide exploration to identify the location of promising spots, and concentrated our investigation near those spots. Table 2 shows the nozzle configurations and range of variables covered in the present study.

Sample Acoustic Results

This section discusses representative acoustic data for each class of deflectors shown in Fig. 4. They are not necessarily the optimal configurations. The acoustic data comprise scaled-up far-field spectra, OASPL, and PNL time histories.

Figure 5 shows typical spectra of Case 2V. At $\theta = 20°$ and 40° we note substantial reductions in the downward emission and sideline emissions, spanning the full-scale frequency range of 200-700 Hz. At $\theta = 60°$ the benefit is small but perceptible, and at $\theta = 90°$ the benefit is practically zero. The OASPL directivities are shown in Fig. 6. The downward and sideline reductions are roughly equal, except around $\theta = 90°$ where the sideline noise becomes slightly elevated. The flyover PNL histories for case 2V are shown in Fig. 7. The downward and sideline PNLs are reduced by about the same amount. The EPNL reductions are 3.6 dB for flyover and 3.3 dB for sideline, giving a cumulative reduction of 6.9 dB.

We now examine the acoustics of the wedge deflector W. Figures 8 and 9 show some fundamental differences between the sound emission of W and that of 2V. The wedge configuration produces substantial noise suppression not only at small polar angles but also at polar angles as large as 70°. There is notable benefit up to $\theta = 100°$ for downward and noise and up to $\theta = 80°$ for sideline noise. Figure 10 shows significant reduction of the peak level of PNL. The EPNL reductions are 4.2 dB for flyover and 3.6 dB for sideline, for a cumulative reduction of 7.7 dB.

The combination of wedge with vanes (2V+W) retains the benefits of the wedge and adds significant reduction in downward noise and moderate reduction in sideline noise. This is evidenced in Figs. 11-13. The EPNL reductions are 5.6 dB for flyover and 3.8 dB for sideline. The cumulative EPNL is thus reduced by 9.3 dB.

The case with two vane pairs (4V) improves mainly downward noise reduction relative to the case with a single pair of vanes (2V). See Figs. 14-16. The

EPNL reductions are 5.0 dB for flyover and 3.3 dB for sideline, for a cumulative reduction of 8.3 dB.

Correlations

To fully explain the noise reduction caused by the deflectors we need to know at a minimum the mean and turbulent velocity fields. Surveys of mean velocity field are ongoing. A rudimentary attempt is made here to correlate the noise reduction with the overall turning of the flow imparted by the deflectors. It is a generalized version of the correlation described by Papamoschou in earlier works on FFD [4].

Each vane pair develops a lift force whose equal and opposite force, **F**, turns the flow in the direction of **F**. See Fig. 17. Let F_j be the magnitude of the turning force of deflector pair j. We define the "turning effort" as the sum of the magnitudes of the turning forces divided by the axial momentum of the secondary (bypass) flow:

$$\epsilon \;=\; \frac{\sum_{j=1}^{N} F_j}{\dot{m}_{\rm s} U_s}$$

The turning effort is thus expressed in terms of an overall deflection angle, ϵ. This angle has physical meaning only when the deflectors produces a unidirectional force, in which case ϵ measures the plume deflection in the direction of the force. Clearly, ϵ does not discriminate on whether the flow is turned downward, sideward, or upward. The understanding here is that all the deflector arrangements turn the flow downward and/or sideward. Thus, all the deflectors are bound to have some impact on the *cumulative* measures of noise, which include the downward and sideline directions. For this reason we will correlate the cumulative OASPL and the cumulative EPNL with ϵ.

A recent computational study of fan flow deflectors allows us to make preliminary estimates of the forces F_j [3]. It was determined that the lift of an airfoil-shaped vane placed inside the convergent fan duct is governed by the dynamic pressure at the leading edge of the vane, $q_{\rm LE}$. The lift slope matches that of an external airfoil, i.e., it is about 6 rad^{-1}. Thus, the force of an individual airfoil-type vane deflectors is

$$F_{vane} \;=\; 6\;\alpha\;q_{\rm LE}\;c\;w$$

where α is the vane angle of attack, c is the vane chord length and w is span of the vane (equal to the local height of the bypass duct). The treatment of the wedge-type deflector is not as straight-forward. Here each side of the wedge is treated as the lower (compression) side of an airfoil. Examination of the pressure coefficients of airfoils at various angles of attack shows that the lower side contributes to roughly one quarter of the total lift. Therefore, each side of the wedge is assumed to have a lift slope of 6/4=1.5 rad^{-1}. The force generated by each side of the wedge is

$$F_{wedge} \;=\; 1.5\;\alpha\;q_s\;h\;\ell$$

where α is the wedge half-angle, q_s is the dynamic pressure of the fan stream at the fan exit, h is the exit height of the fan duct, and ℓ is the side length of the wedge.

It is important to realize that the "turning effort" ϵ, as defined here, is a brute-force metric. It does not account for the azimuthal directionality of the deflector arrangements. Further, it does not consider the fact that, as the vanes move deeper inside the fan duct, their effectiveness in turning the bypass plume declines (the lift force is transmitted to the nozzle walls and not to the plume). Given these shortcomings, we cannot expect good correlations of the noise data. However, the plots may help identify promising arrangements that produce good noise reduction with minimal aerodynamic disturbances.

Figure 18 plots the reduction of cumulative OASPL in the direction of peak emission versus turning effort. Each class of deflectors is identified. There is an overall trend of increasing noise suppression with turning effort, but predictably the scatter is significant. Recalling that the FFD primarily reduces noise from large-scale turbulent noise (which is the main contributor to peak noise), the upward trend of Fig. 18 makes sense. Based on the force definitions discussed earlier, the wedge-type deflectors (W) produce the least turning and the two-vane pair configurations (4V) the most turning.

Figure 19 presents the reduction of cumulative OASPL in the direction $\theta = 45°$. This is an important direction because it corresponds to the occurrence of the maximum PNL. The correlation is very weak, with equal amounts of noise reduction being produced by small and large turning efforts. The figure suggests that the wedge-type deflectors are superior in this regard. As already seen in Fig. 9, they provide very good noise reduction at $\theta = 45°$.

The reduction in cumulative OASPL at $\theta = 90°$ is shown in Fig. 20. Amidst the considerable scatter, there seems to be a trend of declining noise reduction (and even slight noise increase) when ϵ exceeds 0.5°. This is consistent with past observations in

nozzles with vanes at very large angles of attack [1]. The $\theta = 90°$ direction is quite important for EPNL as it affects the "duration correction" of the EPNL metric. Once again, we notice the superiority of the wedge-type defletors. They provide the best OASPL reduction for the least turning effort.

Finally, Fig. 21 presents the reduction in cumulative EPNL. The best reduction in EPNL is achieved by case 2V+W. The overall trend suggests the occurrence of a maximum around $\epsilon = 1°$, although it is too early draw firm conclusions. Such trend could be explained by the opposing trends of peak OASPL and OASPL at $\theta = 90°$ versus ϵ, as suggested by Figs. 18 and 19, respectively. In other words, increasing the turning effort beyond a certain point results in further suppression of the peak OASPL but less suppression, and possibly increase, of the OASPL at $\theta = 90°$.

Conclusion

The present status of a parametric study of fan flow deflectors (FFD) for jet noise suppression has been presented. Reductions in cumulative EPNL as high as 9.6 dB have been measured. Correlations of noise reduction versus a rudimentary metric that describes the turning effort by the deflectors help bring out some general trends and identify promising deflector configurations.

Acknowledgments

The author gratefully acknowledges the support of Goodrich Aerospace, Aerostructures Group. Mr. Ali Dadvar is thanked for conducting the experiments.

References

[1] Papamoschou, D. and Nishi, K.A., "Jet Noise Suppression with Fan Flow Deflectors in Realistic-Shaped Nozzles," AIAA-2005-0993.

[2] Papamoschou, D., "New Method for Jet Noise Suppression in Turbofan Engines," *AIAA Journal*, Vol. 42, No.11, 2004, pp. 2245-2253.

[3] Murayama, T., Papamoschou, D., and Liu, F., "Aerodynamics of Fan Flow Deflectors for Jet Noise Suppression," AIAA-2005-0994.

[4] Papamoschou, D. and Nishi, K.A., "Turbofan Jet Noise Reduction via Deflection of the Bypass Streem," AIAA-2004-0187.

[5] Saiyed, N.H., Mikkelsen, K.L., and Bridges, J.E., "Acoustics and Thrust of Separate-Flow High-Bypass-Ratio Engines," *AIAA Journal*, Vol. 41, No. 3, 2003, pp. 372-378.

[6] Papamoschou, D. "Acoustic Simulation of Hot Coaxial Jets using Cold Helium-Air Mixture Jets," AIAA-2005-0208.

Table 1 Exit flow conditions

Quantity	Core	Fan
Nozzle diameter (mm)	17.0	31.0
Plug diameter (mm)	11.5	-
Height of exit annulus (mm)	2.2	3.1
Lip thickness (mm)	0.8	0.8
Velocity (m/s)	460	334
Mach number	0.86	0.95
Bypass ratio	-	4.8

Table 2 Deflector Configurations

Case	Configuration
Base	Clean nozzle
2V	Single pair of vanes. 56 configurations: Variables: $5 \le \alpha \le 15$ $50 \le \phi \le 150$ $3\text{mm} \le c \le 6\text{mm}$ $1\text{mm} \le x_{\text{te}} \le 3\text{mm}$
W	Wedge. 14 configurations. Variables: $10 \le \alpha \le 25$ $5\text{ mm} \le \ell \le 10\text{ mm}$ $-5\text{ mm} \le x_{\text{te}} \le 4\text{ mm}$
2V+W	Combination wedge with single pair of vanes. 13 configurations. Subsets of above ranges.
4V	Two pairs of vanes. 14 configurations. Variables: $7 \le \alpha_1, \alpha_2 \le 12$ $50 \le \phi_1 \le 90$ $110 \le \phi_2 \le 170$

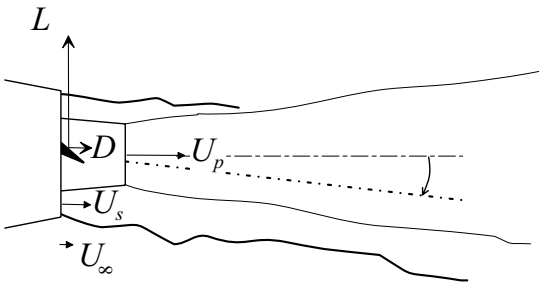

Fig.1 General concept of Fan Flow Deflection (FFD).

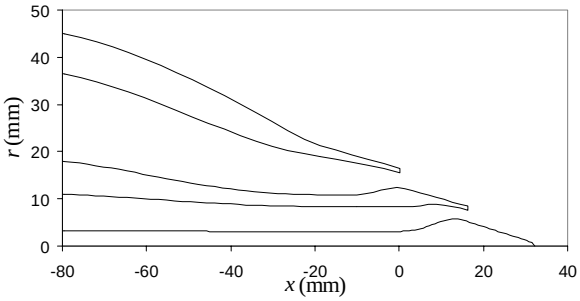

Fig.2 Radial coordinates of UCI nozzle.

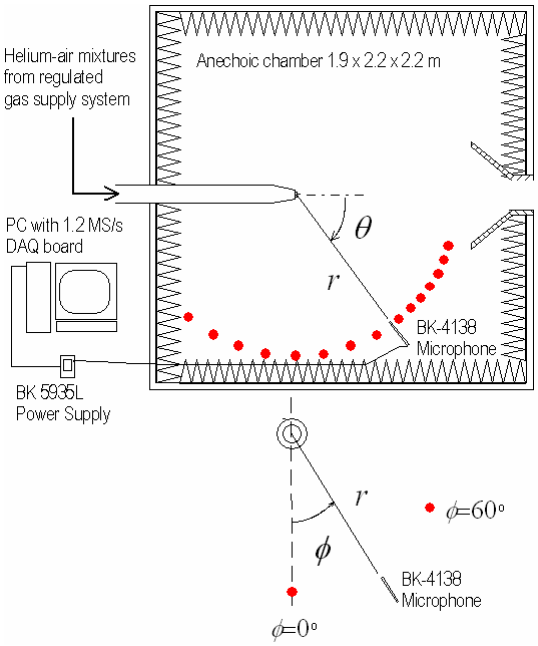

Fig.3 UCI Jet Aeroacoustics Facility.

2V

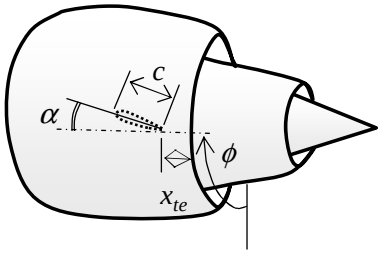

W

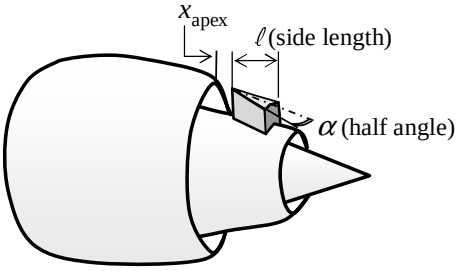

2V+W

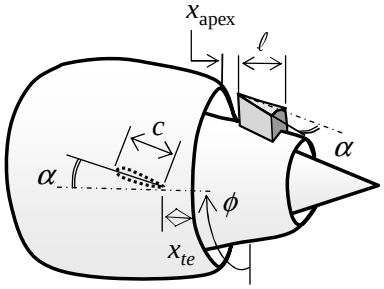

4V

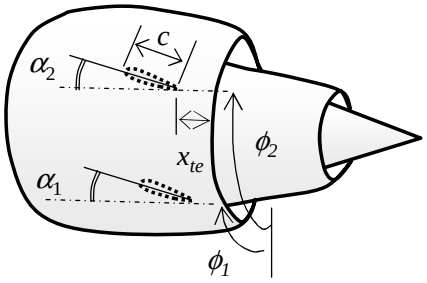

Fig.4 Deflector configurations.

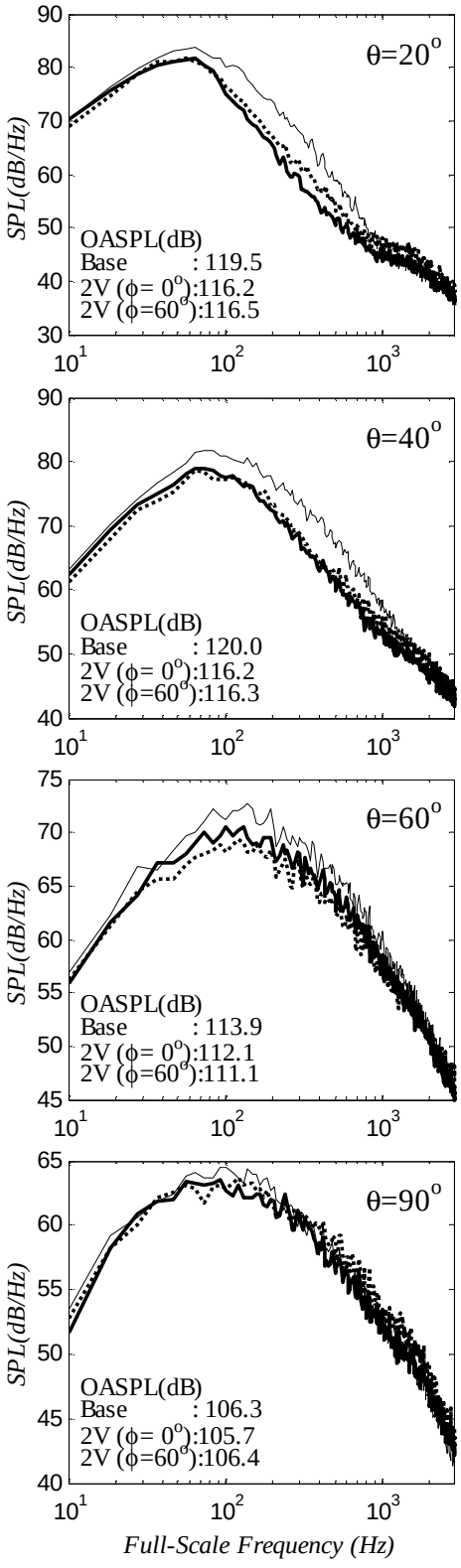

Fig.5 Far field spectra for 2V at various polar angles. Thin line: baseline; thick lines: 2V at microphone azimuth angles 0° (solid) and 60° (dotted).

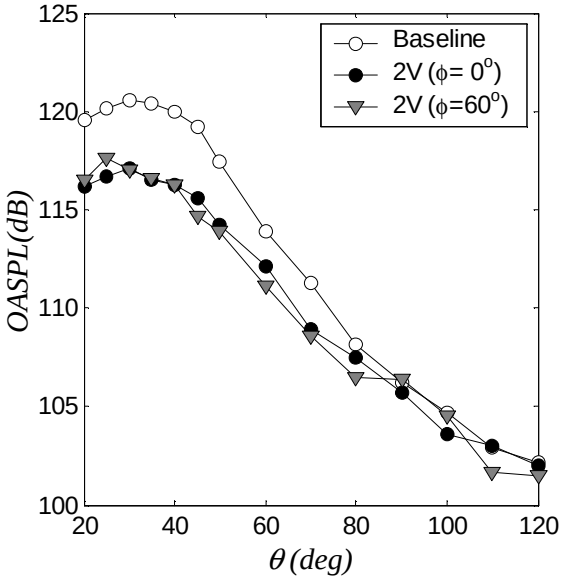

Fig.6 Overall sound pressure levels for 2V at microphone azimuth angles 0° and 60°.

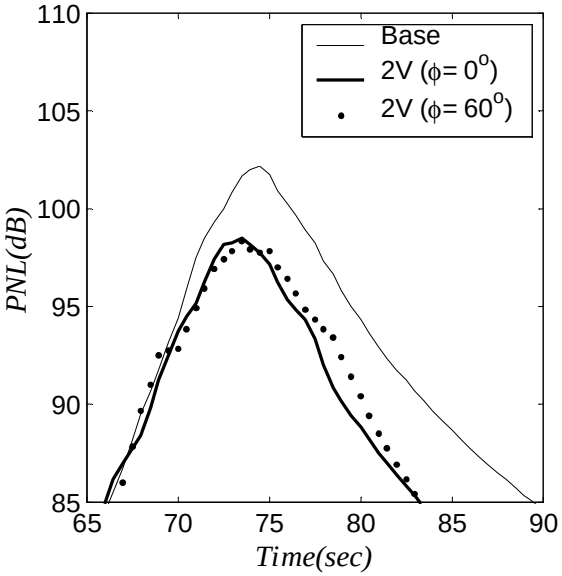

Fig.7 Flyover perceived noise level history for 2V based on microphone azimuth angles 0° and 60°.

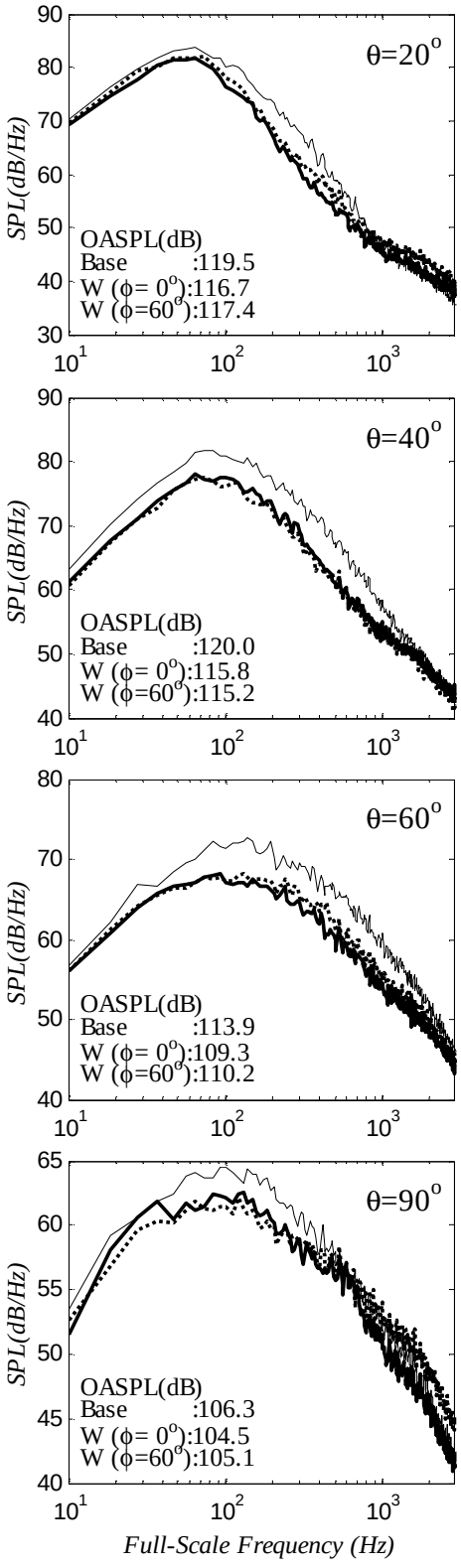

Fig.8 Far field spectra for W at various polar angles. Thin line: baseline; thick lines: W at microphone azimuth angles 0° (solid) and 60° (dotted).

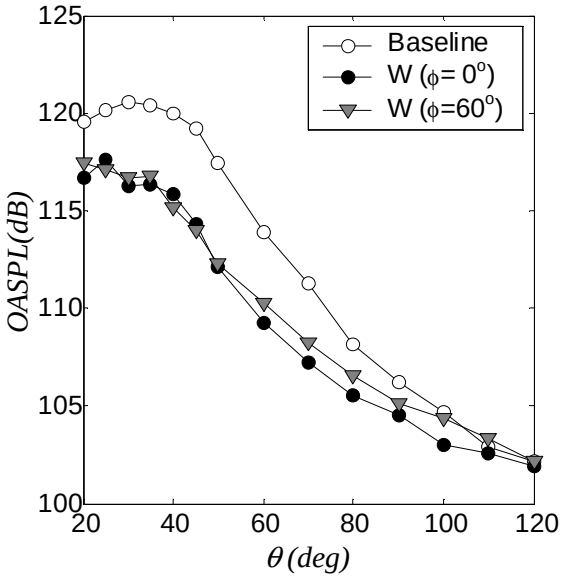

Fig.9 Overall sound pressure levels for W at microphone azimuth angles 0° and 60°.

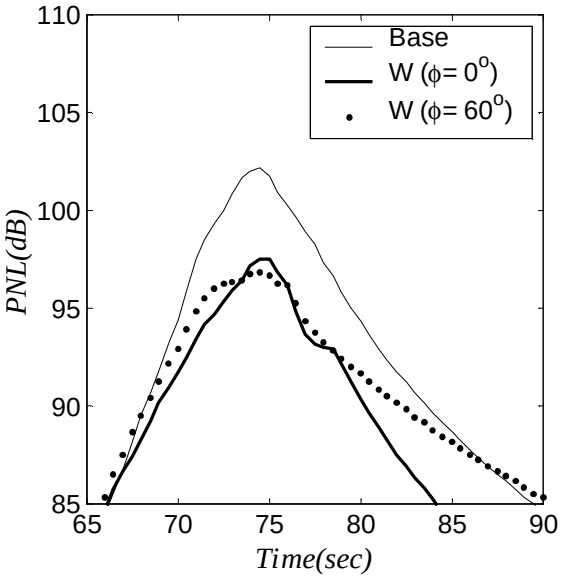

Fig.10 Flyover perceived noise level history for W based on microphone azimuth angles 0° and 60°.

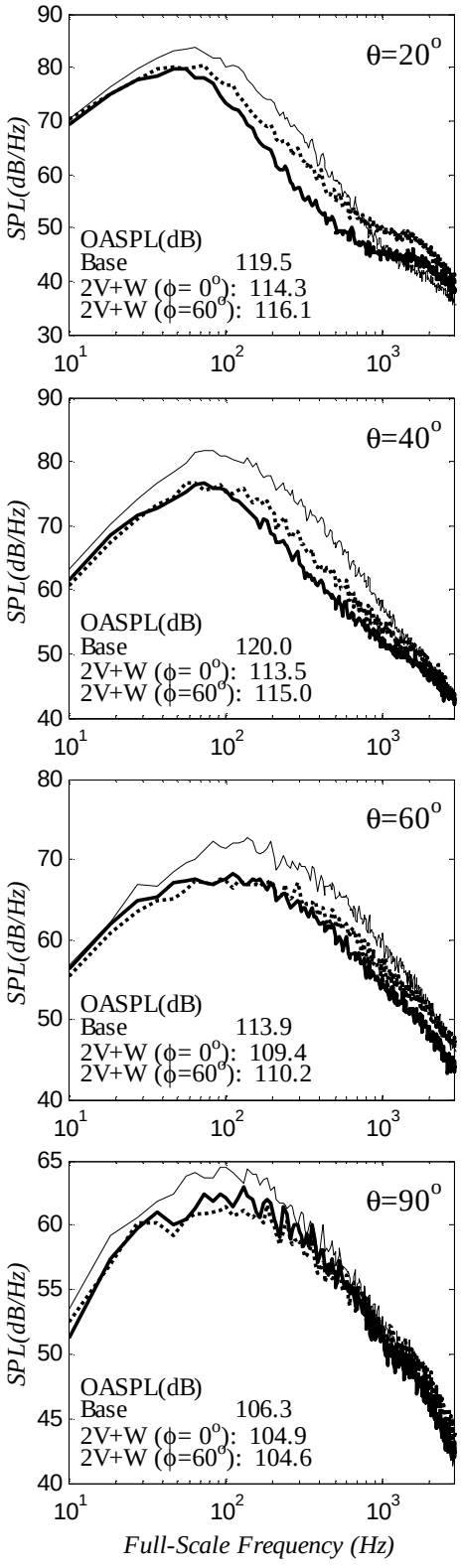

Fig.11 Far field spectra for 2V+W at various polar angles. Thin line: baseline; thick lines: 2V+W at microphone azimuth angles 0° (solid) and 60° (dotted).

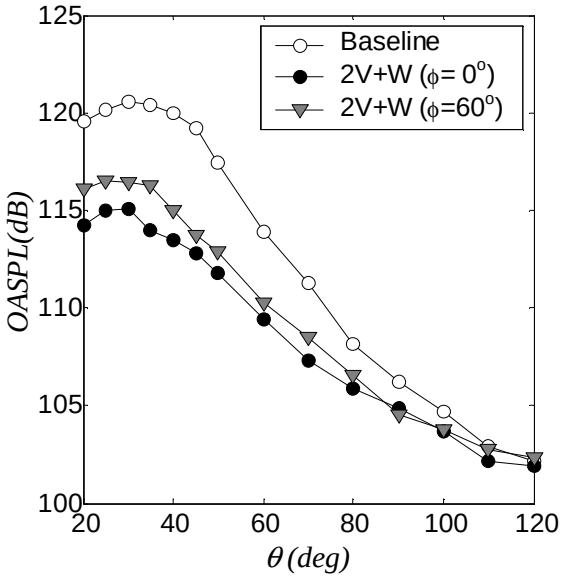

Fig.12 Overall sound pressure levels for 2V+W at microphone azimuth angles 0° and 60°.

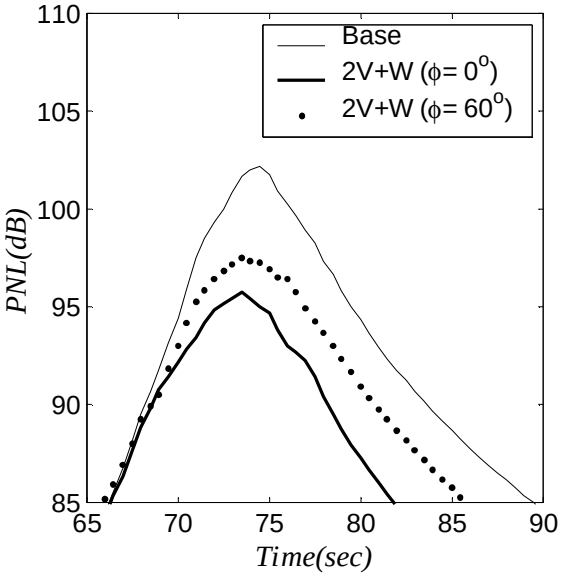

Fig.13 Flyover perceived noise level history for 2V+W based on microphone azimuth angles 0° and 60°.

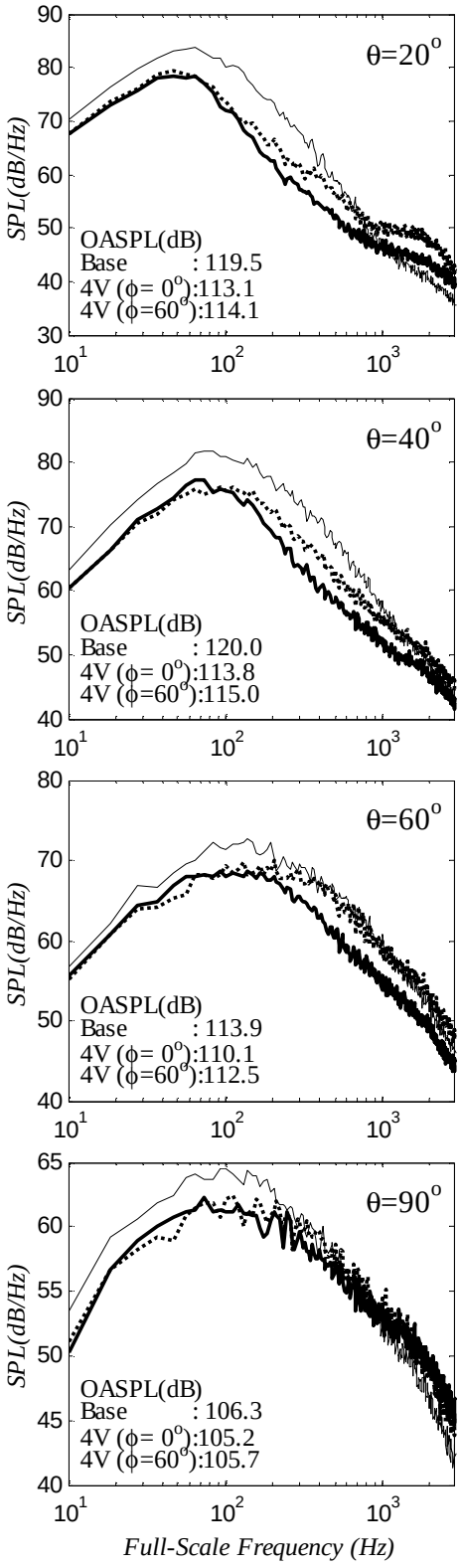

Fig.14 Far field spectra for 4V at various polar angles. Thin line: baseline; thick lines: 4V at microphone azimuth angles 0° (solid) and 60° (dotted).

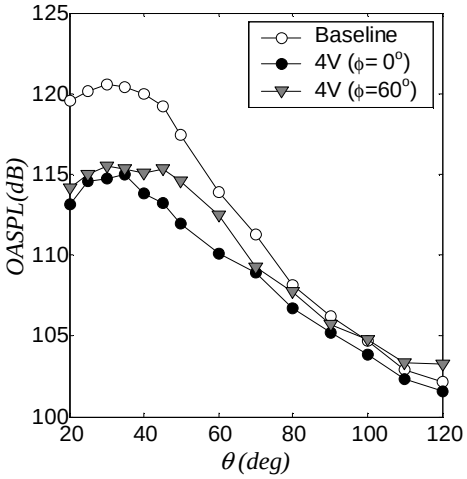

Fig.15 Overall sound pressure levels for case 4V at microphone azimuth angles 0° and 60°.

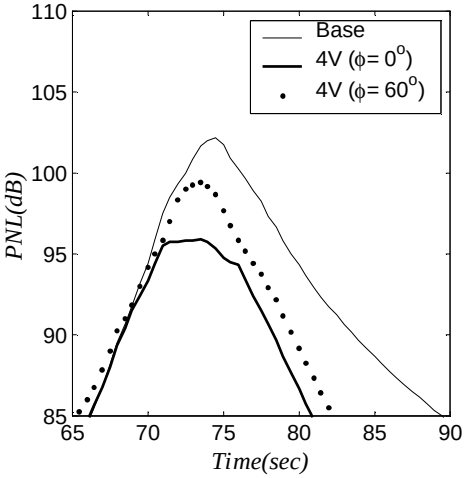

Fig.16 Flyover perceived noise level history for case 4V based on microphone azimuth angles 0° and 60°.

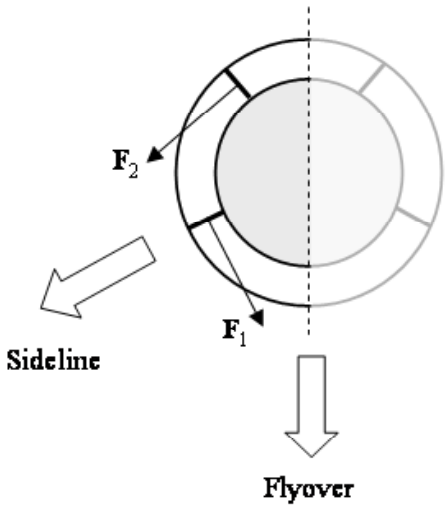

Fig.17 Deflection forces.

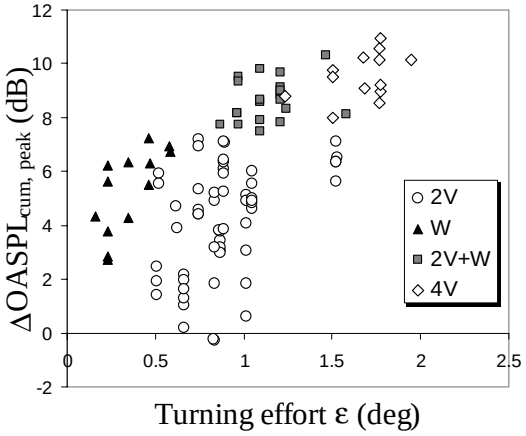

Fig.18 Reduction in cumulative OASPL in the direction of peak emission.

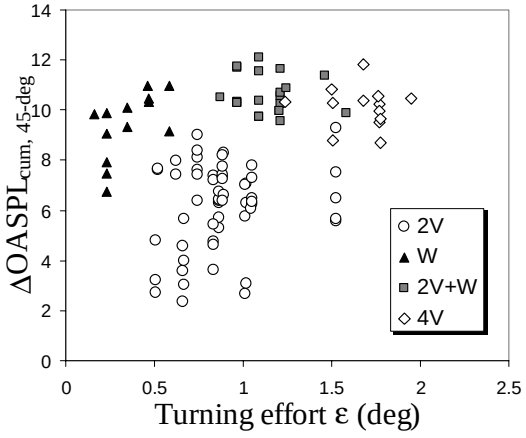

Fig.19 Reduction in cumulative OASPL at $\theta = 45°$.

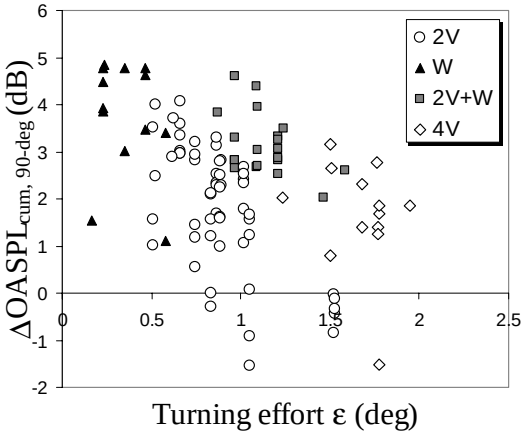

Fig.20 Reduction in cumulative OASPL at $\theta = 90°$.

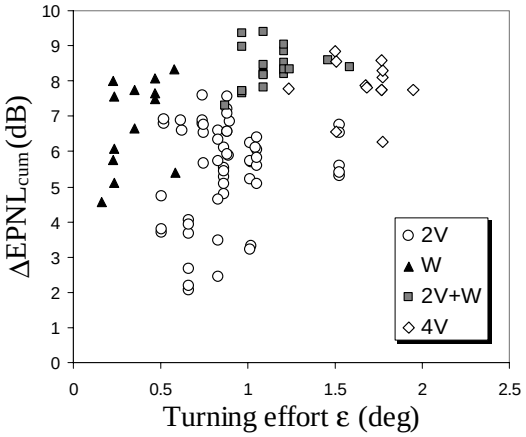

Fig.21 Reduction in cumulative EPNL.